Nanoporous Nitrogen-Doped Graphene Oxide/Nickel Sulfide Composite Sheets Derived from a Metal-Organic Framework as an Efficient Electrocatalyst for Hydrogen and Oxygen Evolution

Kolleboyina Jayaramulu, Justus Masa, Ondrej Tomanec, Daniel Peeters, Vaclav Ranc, Andreas Schneemann, Radek Zboril, Wolfgang Schuhmann, and Roland A. Fischer**

Engineering of controlled hybrid nanocomposites creates one of the most exciting applications in the fields of energy materials and environmental science. The rational design and in situ synthesis of hierarchical porous nanocomposite sheets of nitrogen-doped graphene oxide (NGO) and nickel sulfide (Ni_7S_6) derived from a hybrid of a well-known nickel-based metal-organic framework (NiMOF-74) using thiourea as a sulfur source are reported here. The nanoporous NGO/MOF composite is prepared through a solvothermal process in which Ni(II) metal centers of the MOF structure are chelated with nitrogen and oxygen functional groups of NGO. NGO/Ni_7S_6 exhibits bifunctional activity, capable of catalyzing both the hydrogen evolution reaction (HER) and the oxygen evolution reaction (OER) with excellent stability in alkaline electrolytes, due to its high surface area, high pore volume, and tailored reaction interface enabling the availability of active nickel sites, mass transport, and gas release. Depending on the nitrogen doping level, the properties of graphene oxide can be tuned toward, e.g., enhanced stability of the composite compared to commonly used RuO_2 under OER conditions. Hence, this work opens the door for the development of effective OER/HER electrocatalysts based on hierarchical porous graphene oxide composites with metal chalcogenides, which may replace expensive commercial catalysts such as RuO_2 and IrO_2.

1. Introduction

Hydrogen is one of the most fascinating alternative energy resources to tackle the current energy crisis and environmental issues.[1–4] Especially, electrochemical water splitting, which is composed of two half reactions, the hydrogen evolution reaction (HER) and the oxygen evolution reaction (OER), to produce hydrogen and oxygen, respectively, has been widely considered as an ideal strategy for sustainable mass production of hydrogen to support a global hydrogen economy.[5–9] An ideal bifunctional electrocatalyst entails high electrocatalytic activity with minimum overpotential to produce a large current density for each half reaction with sufficient long-term stability.[10] Precious Pt-based materials as well as noble RuO_2/IrO_2 nanomaterials are known to be efficient HER and OER electrocatalysts, respectively.[11–16] However, commercial scale synthesis of these noble materials faces several challenges due to the high price and scarcity of the materials.

During the past decade, innovation and efforts of material scientists have led to the development of a wide variety of earth-abundant transition metals and carbon-based materials with unprecedentedly promising electrocatalytic properties.[17] Abundant and low-cost nickel sulfide (NiS_x) with intrinsic metallic behavior (continuous Ni—Ni bonds), and high conductivity was recently shown to be an effective and very promising low-cost electrocatalyst for various electrochemical applications.[18] Pristine nickel sulfide has previously been used for

Dr. K. Jayaramulu, Dr. D. Peeters, Dr. A. Schneemann
Inorganic Chemistry II
Ruhr-University Bochum
44801 Bochum, Germany

Dr. K. Jayaramulu, Dr. A. Schneemann, Prof. R. A. Fischer
Chair of Inorganic and Metal-Organic Chemistry
Department of Chemistry and Catalysis Research Centre
Technical University of Munich
85748 Garching, Germany
E-mail: roland.fischer@tum.de

Dr. K. Jayaramulu, O. Tomanec, Dr. V. Ranc, Prof. R. Zboril
Regional Centre of Advanced Technologies and Materials
Faculty of Science
Palacky University Olomouc
Šlechtitelů 27, 783 71 Olomouc, Czech Republic

Dr. J. Masa, Prof. W. Schuhmann
Analytical Chemistry
Center for Electrochemical Sciences (CES)
Faculty of Chemistry and Biochemistry
Ruhr-University Bochum
44780 Bochum, Germany
E-mail: wolfgang.schuhmann@rub.de

The ORCID identification number(s) for the author(s) of this article can be found under https://doi.org/10.1002/adfm.201700451.

DOI: 10.1002/adfm.201700451

electrocatalysis of either the HER or the OER. However, nickel sulfide-based materials that can efficiently catalyze both the OER and the HER have seldom been reported. Furthermore, to achieve highly efficient nanocatalysts with high surface area, a hierarchical porous structure would be beneficial to expose active sites and enhance mass transport of the electrolyte and substrate into the inner layers of the catalyst. Therefore, porous materials are expected to be advantageous. Among the porous materials, metal-organic frameworks (MOFs) have particularly attracted attention due to their inherent properties such as high surface area, large pore volume, active metal sites with ordered and tunable pores.[19–25] As reported previously, nonporous graphene/graphene oxide sheets are becoming inexpensive and have proved to be outstanding support matrices for advanced materials for electrocatalysis and other energy-related applications.[26–33] Hybrids of MOFs and graphene oxide (GO/MOFs) exhibit complementary properties such as large internal surface area with hierarchical pores and high stability.[34–41]

In this work, we report a rational, facile, and simple methodology to fabricate a hybrid of nitrogen-doped graphene oxide/nickel sulfide nanosheets (NGO/Ni_7S_6) as active bifunctional electrocatalyst, originated from a composite of a nickel-based MOF, where the nickel sulfide sheets were stabilized on NGO layers (NGO/MOF), as depicted in **Scheme 1**. Further, a significant advantage of utilizing NGO as support as compared to other 2D materials, is that much more nitrogen-doped sites containing defective pockets are available for coordinating with metal ions. This idea motivated us to prepare a composite catalyst with a high-loading of MOFs on NGO. The NGO/MOF hybrid was prepared using a renowned MOF, NiMOF-74, comprised of Ni(II) and 2,5-dihydroxyterephthalate (DHT), and selectively functionalized NGO. NiMOF-74 provides the unique advantage of coordinative unsaturated metal sites that can be varied without affecting the underlying framework structure. Consequently, NGO sheets provide a platform for the nucleation and growth of MOF crystals, where amine and oxygen functional groups of the NGO act as structure directing and coordination modulating centers for the envisaged nanoscale morphology. The resulting materials, denoted (NGO/Ni_7S_6), can serve as highly active, bifunctional electrocatalyst for both HER and OER.

NiMOF-74 was prepared by mixing nickel ions with DHT and letting them react under solvothermal conditions. In the MOF structure, the Ni^{2+} cations have an octahedral coordination sphere of DHT ligands building up a three-dimensional MOF with one-dimensional hexagonal channels having a pore diameter of 11 Å (Scheme 1a) and a large surface area of 1162 m^2 g^{-1} (Figure 2g).[41–43] The structural integrity of as-synthesized MOF was confirmed by PXRD.

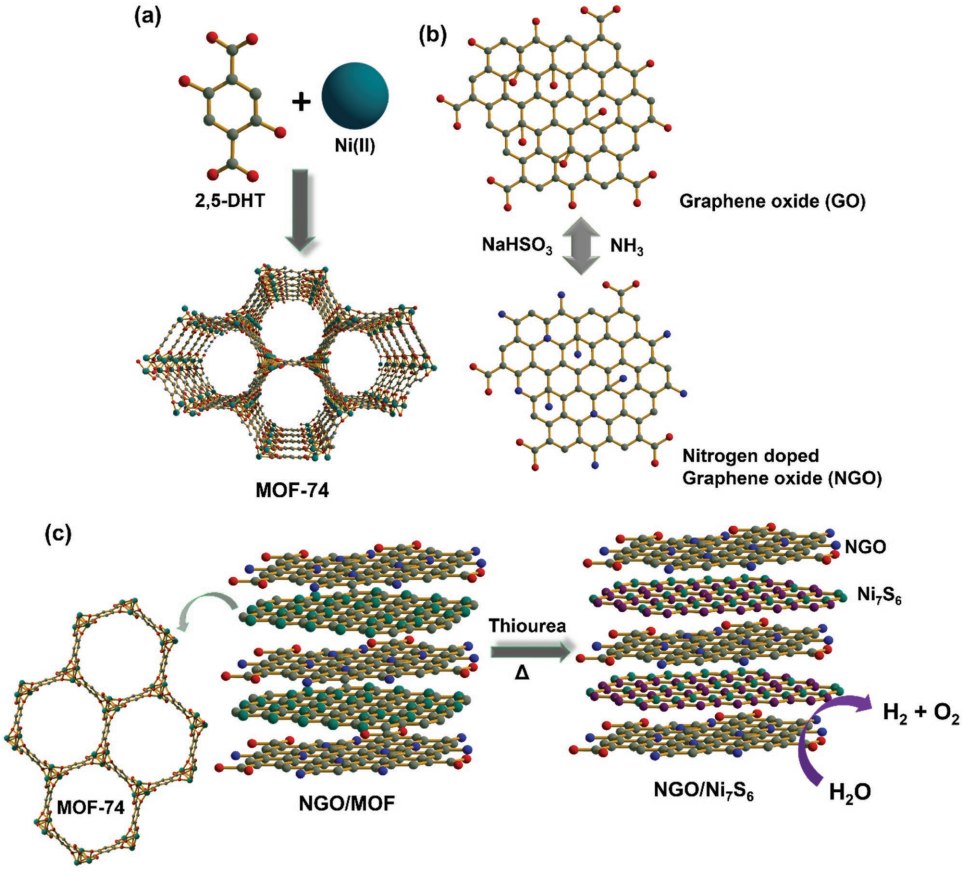

Scheme 1. a) Schematic illustration of the synthesis of an Ni-based metal-organic framework (MOF-74) using Ni(II) and 2,5-dihydroxyterephthalate. b) Selectively amine-functionalized NGO. c) In situ synthesis of 2D NGO and nickel sulfide (NGO/Ni_7S_6) derived from MOF-74 using thiourea as a sulfur source under solvothermal conditions.

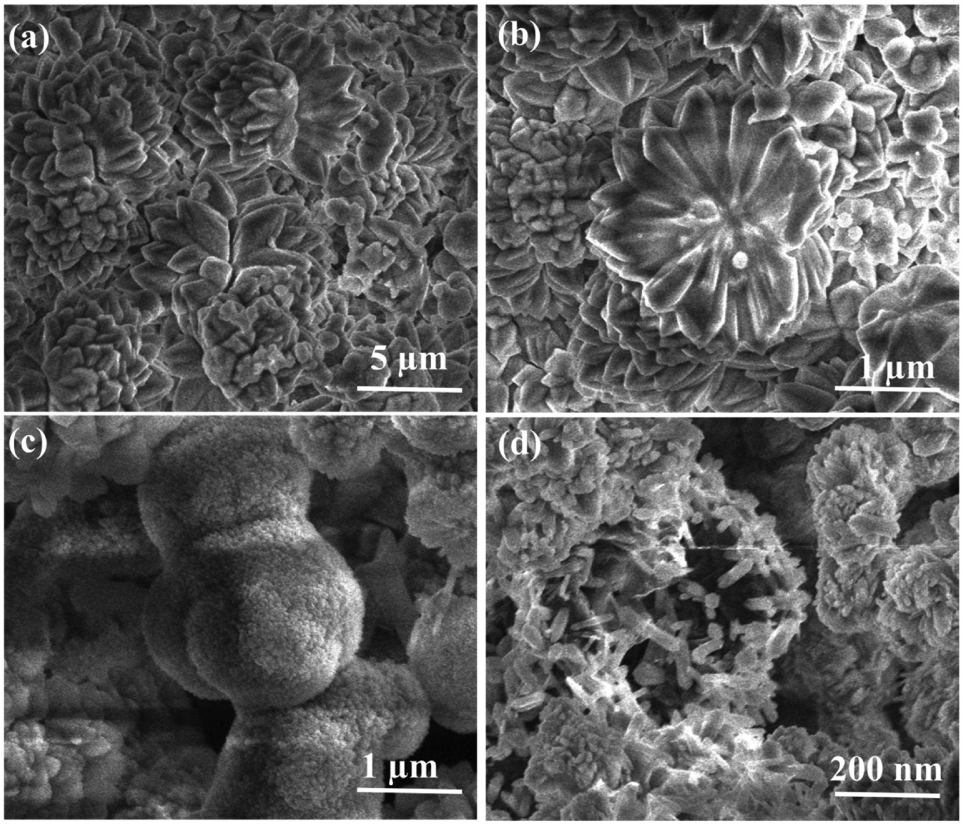

Figure 1. a,b) Scanning electron microscopy (SEM) image of NiMOF-74 showing a flower-like morphology. c,d) NGO/MOF composite microspheres comprised of nanorods.

2. Results and Discussion

The scanning electron microscopy (SEM) images clearly showed the existence of nanospheres/nanorods assembled into flower-like micron particles (**Figure 1**a,b). The NGO was prepared from pristine graphene oxide under hydrothermal conditions through treatment with ammonia and hydrazine monohydrate as shown in Scheme 1b (details in the Supporting Information).[44] The structure, coordination environment, and purity of GO and NGO were characterized through powder X-ray diffraction (PXRD), Raman spectroscopy, and Fourier transform infrared spectroscopy (FT-IR)(Figure S1–S7, Supporting Information). More importantly, the as-synthesized GO contains various oxygen-bearing species including hydroxyl, carboxyl, and epoxy groups. The XRD pattern of NGO reveals typical graphite-related peaks between 20° and 25°. The peak at about 43° is due to disorder of the graphite 101 and 012 plane as typical of GO. The high-resolution N1s X-ray photoelectron spectroscopy (XPS) spectrum reveals different types of nitrogen functionalities including pyridinic, pyrollic nitrogen (Figure S5, Supporting Information). The Raman spectra exhibit a strong D-band (≈1360 cm^{-1}) and G-band (≈1590 cm^{-1}) usually assigned to structural disorder and the graphitized structure, respectively, typical of graphene oxides (Figure S6, Supporting Information). The intensity of the D-band is taken to indicate the presence of defects.

Further, nitrogen adsorption isotherms measured at 77 K of NGO show a nonporous structure with a typical type-II curve and a relatively small surface area of 12 m^2 g^{-1} (Figure S7, Supporting Information). The obtained NGO was used to couple with the MOF to make an NGO and NiMOF-74 hybrid under solvothermal conditions at 100 °C denoted as NGO/MOF (complete experimental procedure is provided in the Supporting Information). The powder X-ray diffraction pattern of NGO/MOF shows all major Bragg reflections that can be indexed to different lattice planes of NiMOF-74 and shows a strong similarity to the simulated XRD pattern of MOF-74 (**Figure 2**a). The XPS spectrum of NGO/MOF shows sharp signals for C, N, O, and Ni atoms (Figure 2c–f). The C 1s signal was deconvoluted into four resolved peaks assigned to four different kinds of carbon atoms, bonded to oxygen, carbon, and nitrogen atoms. The N 1s spectrum shows three peaks attributed to pyrrole, pyridine, and graphitic like nitrogen atoms. Moreover, the Ni 2p core-level spectrum with the Ni $2p_{3/2}$ and Ni $2p_{1/2}$ peaks at 854.1 and 872.0 eV, respectively, indicates the presence of Ni^{2+} in good agreement with literature.[34] Raman analysis of NGO/MOF shows an absorption band positioned at 283 cm^{-1}, which can be assigned to Ni—N vibrations as described previously (Figure 2b).[45] These crystallographic and spectroscopic data support the structural model of successive NGO layers and the coordination of exposed Ni^{2+} cations to nitrogen and oxygen functionalities of NGO. SEM analysis of NGO/MOF shows a bundle of uniform micro-spheres composed of nanorods with a length of ≈200 nm and a very small diameter (10–20 nm) (Figure 1c,d). The shape and morphology

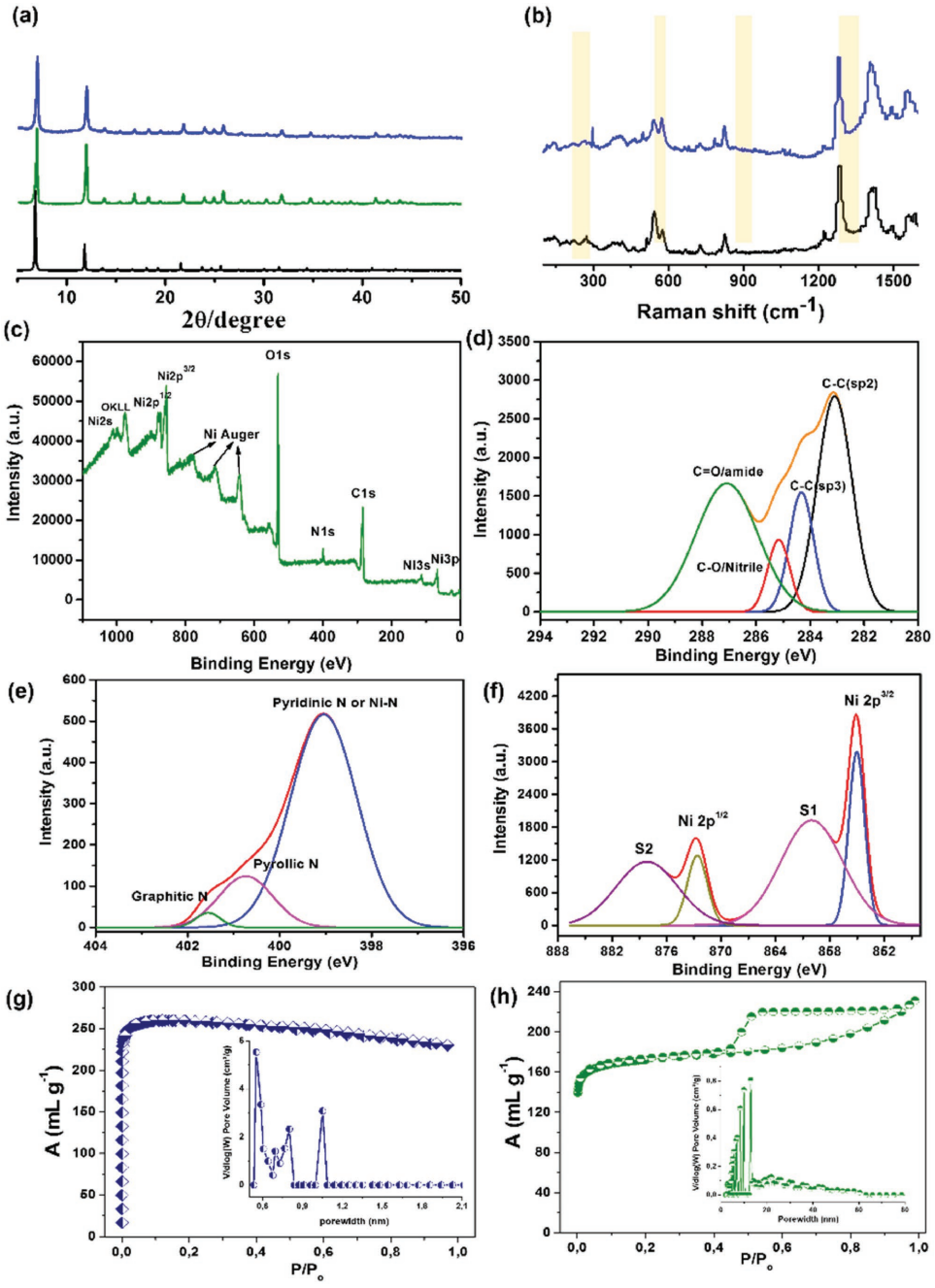

Figure 2. a) Powder XRD patterns of the resulting samples: simulated pattern of MOF-74 (black line); as-synthesized pattern of MOF (green line); prepared hybrid NGO/MOF (blue). b) Raman spectra of pristine MOF-74 (black) and NGO/CPO-27 (blue line). Highlighted are newly formed bands corresponding to nickel-nitrogen as (Ni-N). c) XPS survey spectrum of prepared NGO/MOF hybrid clearly showing the presence of Ni, C, N, and O elements. d) C 1s; e) N 1s; and f) Ni 2p high resolution XPS spectra. Nitrogen adsorption isotherm measured at 77 K. g) MOF-74 showing typical type-I micropore distribution. h) NGO/MOF revealing micro-mesoporous behavior corresponding to type-IV curve with pores in the range of 0.5–60 nm. Insets show pore size distribution calculated using the NLDFT method.

of the composite were completely different from the parental MOF and NGO morphologies. It should be noted that NGO acts as a selective nucleation center for the controlled growth of MOF-74 nanocrystals due to Ni(II) chelation with surface oxygen and nitrogen functionalities at the NGO, thus acting as a structure directing agent. The NGO/MOF exhibits a typical type-IV isotherm characteristic of micro-mesoporous materials with BET and Langmuir surface areas of 770 and 1252 $m^2 g^{-1}$, respectively (Figure 2h). The pore size distribution reveals evidence for pores in the range from 0.5 to 40 nm. The textural parameter (N_2 adsorption isotherm) supports micropores of the MOF, with the remaining pores being likely due to MOF particles binding or chelating with oxygen and nitrogen functional groups of NGO. Encouraged by the result, the synthesized

hierarchical porous NGO/MOF composites were converted into a porous two-dimensional hybrid NGO/Ni_7S_6 nanolayered composite through a sulfidation reaction under hydrothermal conditions using thiourea as a sulfur source. In this process, MOF-74 acts as both sacrificial template and nickel precursor (Scheme 1c).

The composition of the resulting hybrid was confirmed through its powder XRD pattern (**Figure 3**a) in which all the diffraction peaks can be indexed and assigned to the Ni_7S_6 phase (JCPDS Card No. 14-0364). This is consistent with energy dispersive X-ray spectroscopy (EDX) and XPS survey spectrum result as shown in Figures S8 and S9 (Supporting Information). It should be noted that, pristine nickel nitrate was treated with NGO and thiourea under similar conditions, a different cubic pyrite nickel-sulfide NGO/NiS_2 phase was obtained, determined through powder XRD (JCPDS card no. 11–99)[46] (Figure S10a, Supporting Information). Further nitrogen adsorption measurement at 77 K also shows nonporous behavior of hybrid (Figure S10b, Supporting Information). Further, it reveals no residues or contaminants indicating the high purity of the sample. The composition of the NGO/Ni_7S_6 composite was analyzed by XPS (Figure 3d,e). The survey spectrum revealed the expected signals for C, N, O, S, and Ni. The Ni $2p^{3/2}$ peaks at 852.1 and 854.1 eV indicate the presence of divalent and trivalent Ni species in good agreement with literature reports.[34] The S 2p spectrum was deconvoluted into two peaks at 161.8 and 163.2 eV ascribed to S $2p^{3/2}$ and S $2p^{1/2}$, with a broad satellite peak at 169.3 eV corresponding S—O bond.[47,48] The Raman spectrum of the NGO/Ni_7S_6 hybrid shows two intense bands at 1340 (D-band) and 1593 cm^{-1} (G-band). The former is attributed to sp^3 carbon and the latter to graphitic (sp^2) carbon as expected for graphene oxide (Figure S11, Supporting Information). Besides, the BET surface area of NGO/Ni_7S_6 was 132 $m^2\ g^{-1}$ with a large pore volume of 1.09 $cm^3\ g^{-1}$ (Figure S12, Supporting Information). The isotherm shows a typical type-IV curve (H1 type broad hysteresis loop) at higher relative pressure ($P/P_0 > 4$) indicating uniform mesopores. The morphology and chemical composition of the obtained composites were characterized by SEM, transmission electron microscopy (TEM), and EDX elemental mapping. The SEM and TEM images prove the multisheet like 2D structure of the composite with sizes ranging from hundreds of nanometers to a few micrometers (Figures S13–S15 in the Supporting Information and **Figure 4**).[49] A typical HAADF-STEM image of the 2D hybrid shows a uniform distribution of C, N, O, S, and Ni in the whole nanocomposite.

The NGO/Ni_7S_6 composite was tested for electrochemical water splitting in view of its interesting properties, including a high specific surface area, hierarchical meso- and micropores, and active nickel sites, among others.[50–58] The electrocatalytic performance of NGO/Ni_7S_6 for the OER and the HER was evaluated in 0.1 M KOH. Before acquiring any data, catalyst films were first subjected to continuous potential cycling until reproducible voltammograms were obtained. As can be seen in **Figure 5**a, the intensity of the characteristic oxidation of Ni^{2+} ($Ni(OH)_2$) to Ni^{3+} (NiOOH) and of the backward reaction increase with potential cycling, indicating the growth of an oxide/hydroxide layer, which is completed after about 20 CV cycles. The OER performance of NGO/Ni_7S_6 is presented in Figure 5b. For the purpose of comparison, the results are presented together with pristine NGO, the NGO/MOF precursor, and commercial RuO_2, the state-of-the-art benchmark catalyst

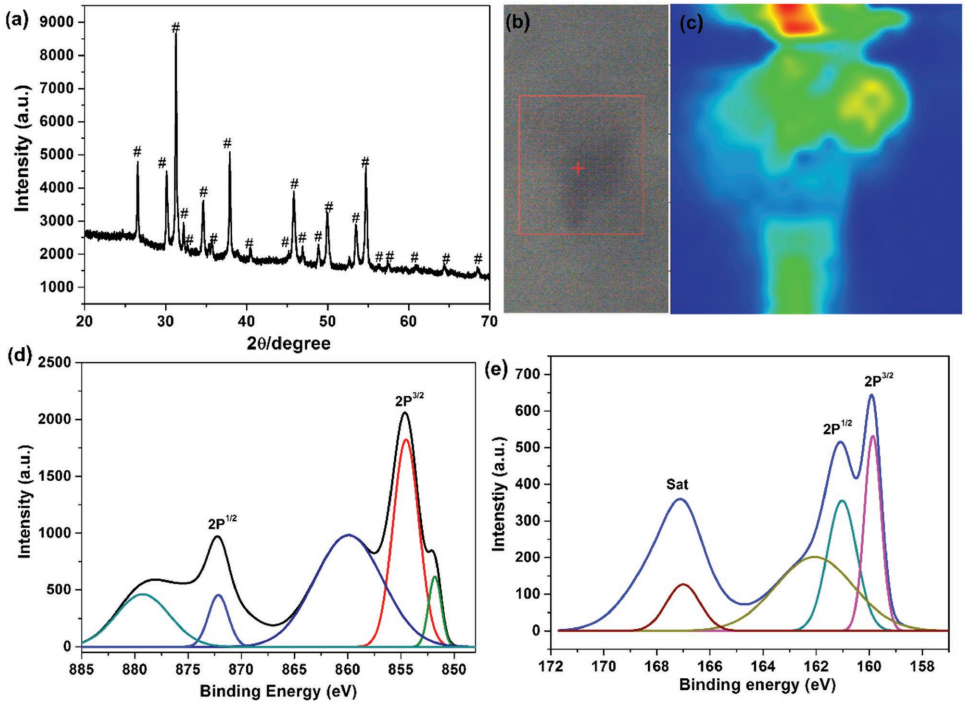

Figure 3. NGO/Ni_7S_6: a) Powder XRD pattern. All peaks marked with # can be indexed and assigned to the Ni7S6 phase (*JCPDS Card No.* 14-0364). b,c) Raman image showing constant D and G bands distribution throughout the sample. d) High-resolution Ni 2p XPS spectrum. e) S 2p XPS spectrum.

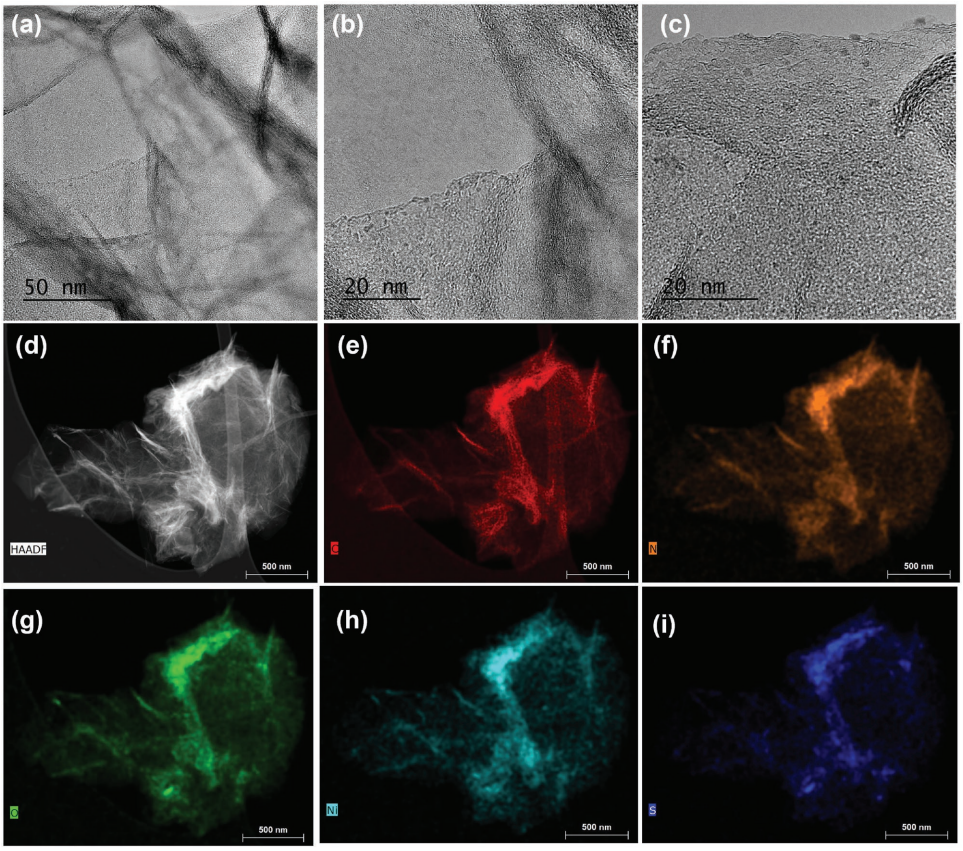

Figure 4. a,c) TEM images of the NGO/Ni_7S_6 nanocomposite revealing evidence of a multisheet morphology; EDS chemical mapping reveals homogeneous distribution of all elements: d) STEM image, e) carbon, f) nitrogen, g) oxygen, h) nickel, and i) sulfide elements throughout the multilayered structure.

for the OER. It is remarkable to note that NGO/Ni_7S_6 exhibits a smaller overpotential for OER than RuO_2. NGO/Ni_7S_6 achieved 10 mA cm^{-2} at 1.61 V as compared to RuO_2, which attained the same current density at 1.62 V. For the precursor composite, NGO/MOF, 10 mA cm^{-2} could not be achieved within the investigated potential window, and the current recorded at 1.61 V was essentially negligible. The oxidation waves prior to oxygen evolution observed in the voltammograms for NGO/Ni_7S_6 and NGO/MOF is due to oxidation of nickel surface species $(HO)Ni^{(II)}$ to $(HOO)Ni^{(III)}$, which is typical of nickel-based oxygen evolution catalysts. The outstanding activity of NGO/Ni_7S_6 accrues from the synergetic interaction between Ni_7S_6 and NGO. The Tafel slope of NGO/Ni_7S_6 was only 45.4 mV dec^{-1}, significantly lower than that for RuO_2 (89.0 mV dec^{-1}) measured under similar conditions (Figure 5b(inset)), and comparable to that of some recently published highly active OER catalysts (**Table 1**). The mechanism for the OER on NGO/Ni_7S_6 thus evidently differs from its mechanism on RuO_2. For a broader perspective of the OER performance of NGO/Ni_7S_6 in relation to other catalysts, its performance was compared against recently reported nonprecious catalysts for the oxygen evolution reaction, as summarized in Table 1.

The HER performance of NGO/Ni_7S_6 was investigated in Ar-saturated 1.0 M KOH by means of linear sweep voltammetry and the results are presented in Figure 5c and compared against the performance of Pt nanoparticles, the state-of-the-art catalyst for HER. The Pt-modified electrode only needed 0.045 V to reach a current density of –10 mA cm^{-2}, whereas NGO/Ni_7S_6 required 0.37 V to attain the same current density. The Tafel slope of the HER on NGO/Ni_7S_6 was 145.5 mV dec^{-1} suggesting a Volmer–Heyrovsky mechanism, while it was 57.5 mV dec^{-1} on Pt, indicating a Volmer–Tafel mechanism. The Volmer–Heyrovsky mechanism is commonly observed for cobalt and nickel-based HER catalysts at alkaline conditions.[10] To further demonstrate the bifunctional nature of NGO/Ni_7S_6, the potential was scanned positive-wards from the HER region to the OER region in argon-saturated KOH (1.0 M), as shown in Figure 5d. The voltage required to perform electrolysis at 10 mA cm^{-2} would correspond to 1.95 V, which is in good agreement with the sum of the overpotentials for the OER and the HER measured individually at the same current density.

Stability measurements for the OER and HER are presented in **Figure 6**. During the stability tests, the electrode was maintained at a rotation speed of 16 000 rpm to prevent the accumulation of gas bubbles on the electrode. Interestingly, during the initial 4 h of the OER (Figure 6a) the electrode gains activity with the potential decreasing from ≈1.75 to 1.59 V. As demonstrated in Figure 5a, an oxide/hydroxide layer, which is the active layer at which the OER proceeds, grows on the catalyst particles and is accompanied by a concomitant increase in activity. After the initial 4 h, the electrode potential continues to decrease, however, much less pronounced. The electrode

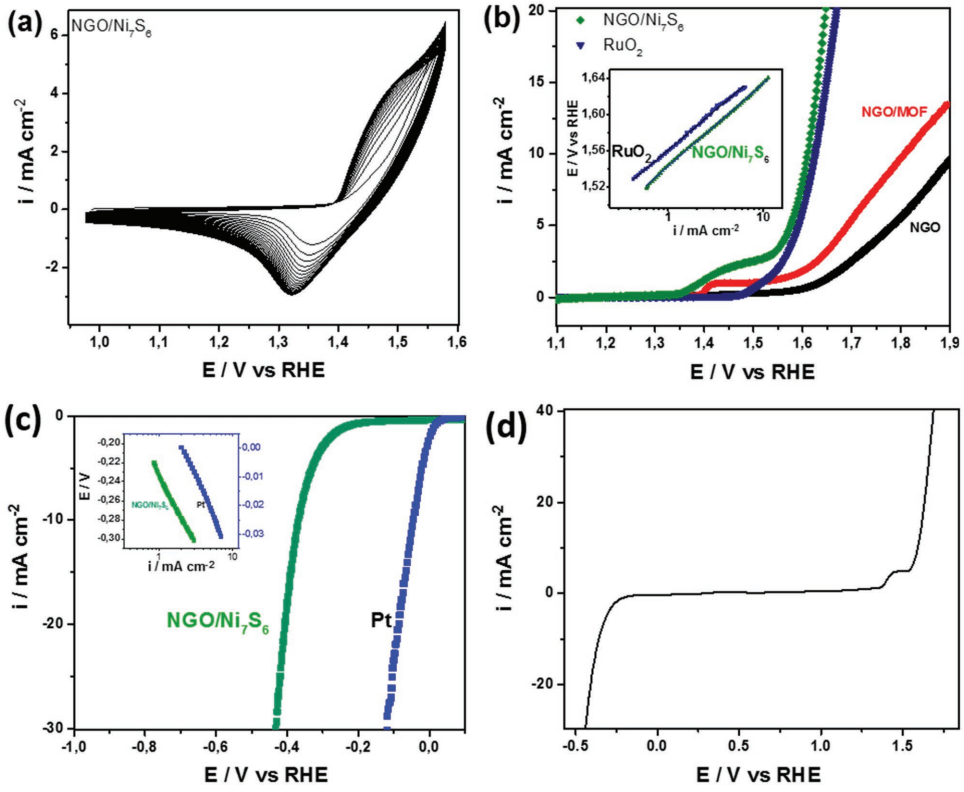

Figure 5. a) Activation of NGO/Ni_7S_6 by continuous potential cycling between 0.95 and 1.60 V at 100 mV s^{-1} in 0.1 M KOH. b) LSVs corrected for the resistance of the electrolyte for the OER of NGO/Ni_7S_6, and of NGO, NGO/MOF, and RuO_2. c) LSVs (iR corrected) for the HER on NGO/Ni_7S_6 plotted together with Pt for comparison, and d) LSV recorded at a scan rate of 10 mV s^{-1} in Ar-saturated 0.1 M KOH with an electrode rotation at 1600 rpm showing both HER and OER.

displayed outstanding stability over 12 h. LSVs recorded before and after 12 h of continuous polarization at 10 mA cm^{-2} (Figure 6a, inset) also show enhanced OER activity after the stability test. The electrode also displayed excellent stability during the HER reaction (Figure 6b). There was no decline in potential during the course of 10 h of galvanostatic polarization of the electrode at –10 mA cm^{-2}, as indicated by the linear sweep voltammetry (LSV) before and after 10 h of polarization.

3. Conclusion

In conclusion, we have successfully demonstrated the fabrication of a nanoporous composite NGO and an Ni-containing metal organic framework (MOF-74). The NGO/MOF composite shows micro-mesoporous behavior, in which micropores originate from the pristine MOF and the mesopores originate from the Ni metal centers, of MOF binding with oxygen and

Table 1. Comparison of the OER performance of NGO/Ni_7S_6 with the activities of selected nonprecious metal catalysts from the literature including state-of-the-art nickel-based catalysts. NCO, nickel cobalt oxide; HNS, hierarchical nanosheets; NR, nanorods; GC, glassy carbon; NF, nickel foam; FTO, fluorine-doped tin oxide; LDH, layered double hydroxide.

Material/substrate	Loading [mg cm^{-2}]	Electrolyte	η [V] 10 mA cm^{-2}	Tafel slope [mV dec^{-1}]	Ref.
NGO/Ni_7S_6	0.21	0.1 M KOH	0.38	45	this work
Ni@NC		0.1 M KOH	0.39	44	[12]
α-$Ni(OH)_2$/GC	0.20	0.1 M KOH	0.33	42	[10]
N-NiFe LDH/NF	0.70	0.1 M KOH	0.23	35	[5]
NCO-HNS/FTO		1.0 M NaOH	0.34	51	[6]
AISI 3014 steel		0.1 M KOH	0.27	66	[7]
Ni_2P/NF	0.14	1.0 M KOH	0.29	47	[8]
Ni_3S_2/NF	37	0.1 M KOH	0.19	159	[9]
α-$Ni(OH)_2$/GC	0.20	0.1 M KOH	0.33	42	[10]
NiFe/NF		0.1 M KOH	0.24	32	[11]
Ni@NC		0.1 M KOH	0.39	44	[12]

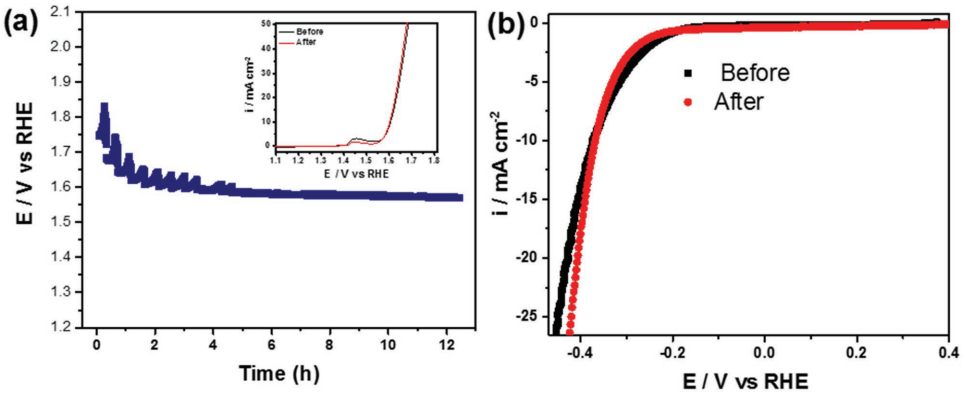

Figure 6. Stability measurements: a) galvanostatic measurements recorded at a current density of 10 mA cm^{-2} on NGO/Ni_7S_6 supported on a graphite RDE electrode in 1.0 M KOH. The electrode was maintained at 1600 rpm to prevent accumulation of gas bubbles. The inset of (a) shows LSVs recorded at a scan rate of 10 mV s^{-1} in 1.0 M KOH during the OER before and after 12 h of constant galvanostatic polarization at 10 mA cm^{-2}. b) LSVs recorded on a graphite electrode modified with NGO/Ni_7S_6 at a scan rate of 5 mV s^{-1} during the HER before and after continuous polarization of the electrode in 1.0 M KOH at –10 mA cm^{-2} for 10 h.

nitrogen functional groups in the NGO structure. In the second step, we successfully converted the NGO/MOF composite to a multisheet 2D nanocomposite (NGO/Ni_7S_6) by treatment with thiourea as a sulfur source. The NGO/Ni_7S_6 composite acts as an ideal bifunctional catalyst for both HER and OER in alkaline solution with great efficiency and high stability. The excellent catalytic activity might be attributed to the synergistic effect between the Ni_7S_6 and NGO in terms of hierarchical porous behavior facilitating fast mass transport, significant textural parameters, the amount of nitrogen, accessible nickel active sites for high electrical conductivity, mass transfer, and stability against corrosion during the HER and OER.

4. Experimental Section

Materials: All reagents and solvents were commercially available and used as supplied without further purification. $Ni(NO_3)_2{\cdot}6\ H_2O$, 2,5-dihydroxyterephthalic acid (DHT), and thiourea were obtained from Aldrich Chemical.

Synthesis of NiMOF-74: Nanocrystals of MOF-74(Ni) were prepared according to a slightly modified procedure from literature.[59] In a 400 mL flask 0.5 g of DHT and 1.5 g of $Ni(NO_3)_2{\cdot}6\ H_2O$ were dissolved in 70 mL dimethylformamide (DMF), 70 mL ethanol, and 70 mL water under sonication. The flask was tightly closed and placed in an oven at 100 °C for 2 d. After cooling to room temperature, the supernatant was decanted and the products were washed three times with DMF, three times with methanol. Methanol as solvent was decanted and replaced once per day during the course of 3 d. The solvent was removed under vacuum and the product was heated under vacuum to 250 °C. After 5 h, the sample was cooled to room temperature and stored under ambient conditions.

Synthesis of GO: GO was prepared using a modified Hummers and Offeman method.[60] In a typical synthesis, 1.5 g of $NaNO_3$ and 1.5 g graphite powder were slowly added to 75 mL conc. H_2SO_4 in an ice bath and allowed to mix properly under constant stirring for 10 min. 10 g $KMnO_4$ were added to this uniform mixture, which was heated by an oil bath (40 °C) under stirring for 0.5 h. Oxidation of graphite occurred and a very viscous dark brown product was formed after 30 min. To this mixture, 75 mL deionized water was added and the temperature of the oil bath was raised to 75 °C. The reactants were stirred at 75 °C for another 15 min. Then 15 mL H_2O_2 (30%) were mixed with 150 mL warm water (≈70 °C) and added to the reaction mixture. The color of the dispersion changed from brown to yellow. The product was centrifuged and washed several times with water. The washed product was dispersed in water and dialysis was performed for 24 h. The dialyzed product was centrifuged to remove excess water and solid product was transferred to a petri dish. The obtained product was stored under vacuum for drying.

Synthesis of NGO: To prepare nitrogen-doped GO[44] the synthesized GO was added into water (0.070 g of GO in 35 mL of H_2O) and treated in an ultrasound bath for 1.0 h. The suspension was centrifuged (5 min; 1000 rpm), and the remaining GO was taken from the stable suspension for subsequent synthesis. Ammonia solution was added into the suspension until a pH value of 10 was reached and then 1.0 mL of monohydrate hydrazine was added under constant stirring. The suspension was placed in a stainless steel autoclave with a Teflon liner, and hydrothermal treatment was carried out at 100 °C for 3 h. Finally, the suspension was centrifuged (5 min; 1000 rpm) and the solid was washed with deionized water and dried at 40 °C for 24 h. The overall yield was about 50%.

Preparation of Hybrid NGO/MOF Nanocomposites: First 100 mg of NGO were dispersed in methanol and sonicated for 5 h. For the synthesis of NGO/MOF-composites, different wt% of NGO solution were added during the preparation of MOF-74(Ni) nanocrystals. The resulting solution was transferred to a Teflon-lined autoclave and placed in an oven at 100 °C for 2 d. The product was washed several times with a water–methanol mixture and dried at 60 °C. The resulting solid composite obtained by variation of the NGO content was denoted by NGO/MOF-74(Ni)-X (N indicates wt% of NGO in comparison to Ni(II) X = 1 (2 wt% N); X = 2 (4 wt% N)).

Preparation of Hybrid NGO/Ni_7S_6 Nanosheets: For the in situ stabilization of nickel sulfide (Ni_7S_6) nanosheets on NGO sheets, the as-prepared 100 mg NGO/MOF-74(X = 1, 2) was added to a teflon bottle containing 200 mg of thiourea in 50 mL methanol and 5 mL water at 200 °C for 24 h. The product was filtered and thoroughly washed with methanol.

Electrochemical Activity Evaluation: All electrochemical measurements were performed in a one-compartment glass cell in the conventional three electrode configuration controlled using a Metrohm-Autolab PGSTAT128N potentiostat/galvanostat. A glassy carbon disk electrode with a geometric area of 0.1134 cm^2 (3.8 mm diameter) was used as working electrode, a platinum cylindrical mesh as counter electrode, and an Ag/AgCl/3 M KCl with a double junction filled with 0.1 M KOH as reference electrode. All measured potentials were converted to the reversible hydrogen electrode (RHE) scale, according to the equation $E_{RHE} = E_{Ag/AgCl} + 0.207 + 0.059pH$.

Catalyst inks were prepared by dispersing the catalyst powder (5 mg) in a mixture of Milli-Q water (490 µL), ethanol (490 µL), and 5% Nafion

(20 µL) followed by ultrasonication for 20 min. A specific volume of the ink was pipetted onto a pre-cleaned glassy carbon electrode to form a catalyst film with a loading equivalent to 0.210 mg cm^{-2}. The resulting films were left to dry in air under ambient conditions for at least 20 min. Before the OER measurements, the modified electrodes were first subjected to continuous potential cycling in the potential window from 1.0 to 1.6 V versus RHE until reproducible voltammograms were obtained. Electrochemical impedance spectroscopy was then recorded at the corresponding open-circuit potential of the electrode, using an ac perturbation of 10 mV_{pp} in the frequency range from 50 kHz to 1 Hz. The resistance of the solution was determined from the resulting Nyquist plot, and later used for ohmic drop correction according to the relation $E_c = E - iRs$, where E_c is the corrected potential and E is the applied potential. The OER activity was recorded by LSV from 1.0 to 2.0 V at a scan rate of 10 mV s^{-1} in oxygen-saturated KOH (0.1 M) with an electrode rotation at 1600 rpm to minimize the accumulation of gas bubbles. Hydrogen evolution measurements were carried out in argon-saturated 1.0 M KOH at scan rate of 5 mV s^{-1} with an electrode rotation at 1600 rpm. Evaluation of the long-term stability of the catalysts was performed chronopotentiometrically in air-saturated KOH (1.0 M) at a current density of 10 mA cm^{-2}, during which the electrode was rotated at 1600 rpm. For the stability measurements, the catalysts were supported on graphite rotating disk (RD) electrodes of 0.19625 cm^2 geometric area, 5.0 mm diameter.

Supporting Information

Supporting Information is available from the Wiley Online Library or from the author.

Acknowledgements

K.J.R. is grateful to the Alexander von Humboldt (AvH) foundation for a postdoctoral fellowship. J.M. and W.S. acknowledge support by the BMBF (NeMeZu; FKZ 03SF0497B). The authors gratefully acknowledge the support from the Ministry of Education, Youth and Sports of the Czech Republic (LO1305) and the assistance provided by the Research Infrastructure NanoEnviCz, supported by the Ministry of Education, Youth and Sports of the Czech Republic under Project No. LM2015073. The authors acknowledge the support by the Operational Programme Research, Development and Education-European Regional Development Fund, project no. CZ. 02.1.01/0.0/0.0/15_003/0000416 of the Ministry of Education, Youth and Sports of Czech Republic.

Conflict of Interest

The authors declare no conflict of interest.

Keywords

electrocatalysis, metal-organic framework (MOF), nanosheets, nickel sulfide, nitrogen-doped graphene oxide

Received: January 24, 2017
Revised: April 21, 2017
Published online:

[1] M. S. Dresselhaus, I. L. Thomas, *Nature* **2001**, *414*, 332.
[2] N. S. Lewis, D. G. Nocera, *Proc. Natl. Acad. Sci. USA* **2006**, *103*, 15729.
[3] J. Greeley, T. F. Jaramillo, J. Bonde, I. Chorkendorff, J. K. Norskov, *Nat. Mater.* **2006**, *5*, 909.
[4] L.-L. Feng, G. Yu, Y. Wu, G.-D. Li, H. Li, Y. Sun, T. Asefa, W. Chen, X. Zou, *J. Am. Chem. Soc.* **2015**, *137*, 14023.
[5] O. Khaselev, J. A. Turner, *Science* **1998**, *280*, 425.
[6] T. F. Jaramillo, K. P. Jørgensen, J. Bonde, J. H. Nielsen, S. Horch, I. Chorkendorff, *Science* **2007**, *317*, 100.
[7] D. V. Esposito, S. T. Hunt, A. L. Stottlemyer, K. D. Dobson, B. E. McCandless, R. W. Birkmire, J. G. Chen, *Angew. Chem. Int. Ed.* **2010**, *49*, 9859.
[8] J. Chang, Y. Xiao, M. Xiao, J. Ge, C. Liu, W. Xing, *ACS Catal.* **2015**, *5*, 6874.
[9] Y. Wang, K. Jiang, H. Zhang, T. Zhou, J. Wang, W. Wei, Z. Yang, X. Sun, W.-B. Cai, G. Zheng, *Adv. Sci.* **2015**, *2*, 1500003.
[10] J. Masa, P. Weide, D. Peeters, I. Sinev, W. Xia, Z. Sun, C. Somsen, M. Muhler, W. Schuhmann, *Adv. Energy Mater.* **2016**, *6*, 1502313.
[11] P. Du, R. Eisenberg, *Energy. Environ. Sci.* **2012**, *5*, 6012.
[12] R. Subbaraman, D. Tripkovic, K.-C. Chang, D. Strmcnik, A. P. Paulikas, P. Hirunsit, M. Chan, J. Greeley, V. Stamenkovic, N. M. Markovic, *Nat. Mater.* **2012**, *11*, 550.
[13] I. E. L. Stephens, I. Chorkendorff, *Angew. Chem. Int. Ed.* **2011**, *50*, 1476.
[14] E. Tsuji, A. Imanishi, K.-i. Fukui, Y. Nakato, *Electrochim. Acta* **2011**, *56*, 2009.
[15] Y. Lee, J. Suntivich, K. J. May, E. E. Perry, Y. Shao-Horn, *J. Phys. Chem. Lett.* **2012**, *3*, 399.
[16] M. W. Louie, A. T. Bell, *J. Am. Chem. Soc.* **2013**, *135*, 12329.
[17] X. Zou, Y. Zhang, *Chem. Soc. Rev.* **2015**, *44*, 5148.
[18] X.-Y. Yu, L. Yu, H. B. Wu, X. W. Lou, *Angew. Chem. Int. Ed.* **2015**, *54*, 5331.
[19] S. Bureekaew, S. Horike, M. Higuchi, M. Mizuno, T. Kawamura, D. Tanaka, N. Yanai, S. Kitagawa, *Nat. Mater.* **2009**, *8*, 831.
[20] H.-C. Zhou, J. R. Long, O. M. Yaghi, *Chem. Rev.* **2012**, *112*, 673.
[21] N. Stock, S. Biswas, *Chem. Rev.* **2012**, *112*, 933.
[22] O. Shekhah, H. Wang, M. Paradinas, C. Ocal, B. Schupbach, A. Terfort, D. Zacher, R. A. Fischer, C. Woll, *Nat. Mater.* **2009**, *8*, 481.
[23] W. Xia, A. Mahmood, R. Zou, Q. Xu, *Energy Environ. Sci.* **2015**, *8*, 1837.
[24] K. Jayaramulu, K. K. R. Datta, M. V. Suresh, G. Kumari, R. Datta, C. Narayana, M. Eswaramoorthy, T. K. Maji, *ChemPlusChem* **2012**, *77*, 743.
[25] G. Kumari, K. Jayaramulu, T. K. Maji, C. Narayana, *J. Phys. Chem. A* **2013**, *117*, 11006.
[26] T. Szabó, O. Berkesi, P. Forgó, K. Josepovits, Y. Sanakis, D. Petridis, I. Dékány, *Chem. Lett.* **2006**, *18*, 2740.
[27] T. Szabó, E. Tombácz, E. Illés, I. Dékány, *Carbon* **2006**, *44*, 537.
[28] S. Guo, S. Dong, E. Wang, *ACS Nano* **2010**, *4*, 547.
[29] H. Wang, J. T. Robinson, G. Diankov, H. Dai, *J. Am. Chem. Soc.* **2010**, *132*, 3270.
[30] T. Jiang, Y. Song, D. Du, X. Liu, Y. Lin, *ACS Sens.* **2016**, *1*, 717.
[31] M. Liu, Y. Lu, W. Chen, *Adv. Funct. Mater.* **2013**, *23*, 1289.
[32] B. Luo, S. Liu, L. Zhi, *Small* **2012**, *8*, 630.
[33] A. A. Balandin, S. Ghosh, W. Bao, I. Calizo, D. Teweldebrhan, F. Miao, C. N. Lau, *Nano Lett.* **2008**, *8*, 902.
[34] K. Jayaramulu, K. K. R. Datta, C. Rösler, M. Petr, M. Otyepka, R. Zboril, R. A. Fischer, *Angew. Chem. Int. Ed.* **2016**, *55*, 1178.
[35] M. Jahan, Z. Liu, K. P. Loh, *Adv. Funct. Mater.* **2013**, *23*, 5363.
[36] R. Kumar, K. Jayaramulu, T. K. Maji, C. N. R. Rao, *Chem. Commun.* **2013**, *49*, 4947.
[37] P. Cubillas, M. W. Anderson, M. P. Attfield, *Chem. Eur. J.* **2012**, *18*, 15406.
[38] C. Petit, T. J. Bandosz, *Adv. Mater.* **2009**, *21*, 4753.
[39] C. Petit, B. Mendoza, T. J. Bandosz, *Langmuir* **2010**, *26*, 15302.

[40] Q.-L. Zhu, W. Xia, T. Akita, R. Zou, Q. Xu, *Adv. Mater.* **2016**, *28*, 6391.
[41] K. M. Choi, H. M. Jeong, J. H. Park, Y.-B. Zhang, J. K. Kang, O. M. Yaghi, *ACS Nano* **2014**, *8*, 7451.
[42] S. Gadipelli, J. Ford, W. Zhou, H. Wu, T. J. Udovic, T. Yildirim, *Chem. Eur. J.* **2011**, *17*, 6043.
[43] Z. Li, G. Zhu, G. Lu, S. Qiu, X. Yao, *J. Am. Chem. Soc.* **2010**, *132*, 1490.
[44] Q. He, Q. Li, S. Khene, X. Ren, F. E. López-Suárez, D. Lozano-Castelló, A. Bueno-López, G. Wu, *J. Phys. Chem. C* **2013**, *117*, 8697.
[45] H.-J. Himmel, L. Manceron, *Dalton Trans.* **2005**, *2005*, 2615.
[46] S. L. Yang, H.-B. Yao, M.-R. Gao, S.-H. Yu, *CrystEngComm* **2009**, *11*, 1383.
[47] Z. Wang, P. Li, Y. Chen, J. He, W. Zhang, O. G. Schmidt, Y. Li, *Nanoscale* **2014**, *6*, 7281.
[48] Z. Yang, Z. Yao, G. Li, G. Fang, H. Nie, Z. Liu, X. Zhou, X. a. Chen, S. Huang, *ACS Nano* **2012**, *6*, 205.
[49] Z. Wang, Q. Li, F. Besenbacher, M. Dong, *Adv. Mater.* **2016**, *28*, 10224.
[50] S. Chen, J. Duan, P. Bian, Y. Tang, R. Zheng, S.-Z. Qiao, *Adv. Energy Mater.* **2015**, *5*, 1500936.
[51] H.-Y. Wang, Y.-Y. Hsu, R. Chen, T.-S. Chan, H. M. Chen, B. Liu, *Adv. Energy Mater.* **2015**, *5*, 1500091.
[52] H. Schafer, S. Sadaf, L. Walder, K. Kuepper, S. Dinklage, J. Wollschlager, L. Schneider, M. Steinhart, J. Hardege, D. Daum, *Energy Environ. Sci.* **2015**, *8*, 2685.
[53] T. Zhang, J. Du, P. Xi, C. Xu, *ACS App. Mater. Interfaces* **2017**, *9*, 362.
[54] L.-A. Stern, L. Feng, F. Song, X. Hu, *Energy Environ. Sci.* **2015**, *8*, 2347.
[55] W. Zhou, X.-J. Wu, X. Cao, X. Huang, C. Tan, J. Tian, H. Liu, J. Wang, H. Zhang, *Energy Environ. Sci.* **2013**, *6*, 2921.
[56] M. Gao, W. Sheng, Z. Zhuang, Q. Fang, S. Gu, J. Jiang, Y. Yan, *J. Am. Chem. Soc.* **2014**, *136*, 7077.
[57] X. Lu, C. Zhao, *Nat. Commun.* **2015**, *6*, 6616.
[58] J. Ren, M. Antonietti, T.-P. Fellinger, *Adv. Energy Mater.* **2015**, *5*, 1401660.
[59] T. Grant Glover, G. W. Peterson, B. J. Schindler, D. Britt, O. Yaghi, *Chem. Eng. Sci.* **2011**, *66*, 163.
[60] W. S. Hummers, R. E. Offeman, *J. Am. Chem. Soc.* **1958**, *80*, 1339.